minerals

MDPI

Article

Stylolites in Carbonate Rocks: Morphological Variability According to the Host Rock Texture

Silvana Magni [1], Juan Diego Martín-Martín [2], Paul D. Bons [3] and Enrique Gomez-Rivas [2,*]

[1] Institute of Geology and Paleontology, Charles University, Albertov 6, 128 43 Prague, Czech Republic; magnis@natur.cuni.cz
[2] Departament de Mineralogia, Petrologia i Geologia Aplicada, Facultat de Ciències de la Terra, Universitat de Barcelona, Martí i Franquès s/n, 08028 Barcelona, Spain; juandiegomartin@ub.edu
[3] Department of Geosciences, University of Tubingen, Schnarrenbergstr. 94–96, 72076 Tubingen, Germany; paul.bons@uni-tuebingen.de
* Correspondence: e.gomez-rivas@ub.edu; Tel.: +34-934021408

Abstract: Stylolites are ubiquitous structures in carbonates that present a variety of morphologies. Besides being important structures in terms of rock compaction and deformation, stylolites control limestone permeability, which is influenced by their morphology and arrangement in connected networks. This study characterizes stylolite morphological parameters, such as length, thickness, filling by insoluble material, spacing and connectivity, to provide quantitative data on the relationships between stylolite morphology and carbonate host rock textures. A collection of thin sections from a variety of lithologies and geological settings was analyzed, showing that the stylolite length, thickness and morphology are interrelated and are controlled by the host rock textures. The results show that stylolite linearity, calculated as the ratio between the straight length and the length measured along the stylolite trace, varies according to the stylolite type. Higher stylolite thickness is observed in mud-dominated textures compared to grain-dominated ones but is independent of the stylolite type. There is no clear trend in terms of the amount of insoluble material collected by the stylolites and the rock texture or stylolite type. Analysis of stylolite spacing reveals that heterogeneity in grain size, grain sorting and composition controls stylolite formation.

Keywords: stylolite; rock texture; permeability; morphological analysis; chemical compaction

Academic Editors: Santanu Banerjee and Juan Gómez-Barreiro

Received: 13 December 2024
Revised: 16 January 2025
Accepted: 22 January 2025
Published: 29 January 2025

Citation: Magni, S.; Martín-Martín, J.D.; Bons, P.D.; Gomez-Rivas, E. Stylolites in Carbonate Rocks: Morphological Variability According to the Host Rock Texture. *Minerals* **2025**, *15*, 132. https://doi.org/10.3390/min15020132

1. Introduction

Stylolites are rough dissolution surfaces that form by pressure solution during chemical compaction [1–3]. They can be the result of localized stress-induced dissolution during burial compaction to form so-called bedding-parallel, sedimentary or diagenetic stylolites or by tectonic compression to form tectonic stylolites, which are normally not parallel to bedding. Stylolites are present in many rock types [4,5], but they are particularly common in limestones due to the high solubility and fast reaction kinetics of calcite and other carbonate minerals [6–8]. The dissolution of carbonate rocks typically leads to an enrichment in insoluble material, especially clays and oxides, along the stylolite surfaces [2,9,10]. Interest in stylolites started with the work of Stockdale [1], who found that the material filling stylolite surfaces is the residue that remains after the dissolution of limestone and proposed that the length of stylolite teeth is proportional to the thickness of the dissolved rock volume.

A range of studies suggest that stylolites can affect the permeability of the host rocks, with permeability varying depending on the directions (i.e., parallel versus perpendicular

to the stylolite). In this regard, stylolites can potentially act as barriers to fluids across them [11–13], but also as conduits for fluids along them [14–20]. Other studies have pointed out that stylolites can simultaneously present both types of behaviour [21] or change their role from barriers to conduits (or vice versa) during the geological history of a basin [22,23]. Stylolites can also determine reservoir quality [17,24,25].

Stylolites may have a range of morphologies, from smooth to extremely rough surfaces. Different classifications of stylolite morphologies have been proposed [13,26–28]. The most recent classification of stylolite morphologies is that of Koehn et al. [29], who defined four types: rectangular layer-, seismogram pinning-, suture and sharp peak- and wave-like types (Figure 1a). This classification allows distinguishing between stylolites that grow linearly and non-linearly and is useful for estimating the influence of stylolite on the local permeability variations in rocks [29]. Accordingly, the present study follows this classification.

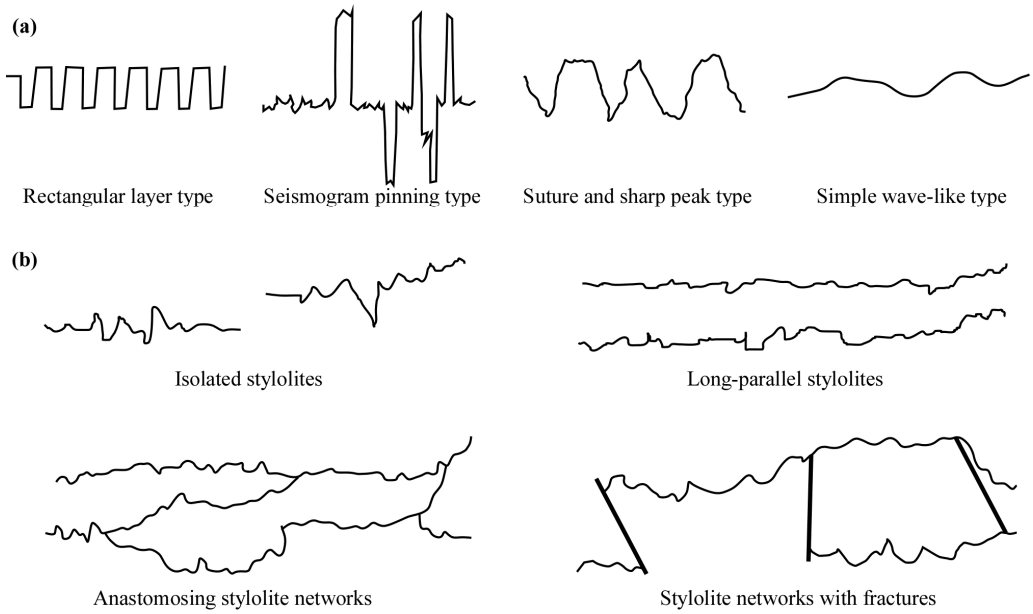

Figure 1. (**a**) Classification of stylolites according to Koehn et al. [29] (figure modified from [29]). (**b**) Types of stylolite connectivity (Figure modified from [9]).

With some exceptions [9,23,30], most studies have analyzed stylolites in isolation. However, the degree of stylolite connectivity is an important parameter, and it is useful for evaluating the potential circulation of fluids through a stylolite-bearing rock. Three types of stylolite connectivity have been identified [9]: (1) isolated stylolites; (2) long-parallel stylolites (not cross-cutting); and (3) (anastomosing) networks of connected stylolites that enclose lenses of the host rock (Figure 1b). Connectivity between stylolites depends not only on their morphology but also on other factors such as their wavelength, amplitude and orientation.

A key question about stylolites is what factors determine their morphology. A variety of parameters has been considered, including the rock texture [2,29–32], grain size and grain size distribution [33–35] and clay content [34,36], among others. The presence of clays was suggested to be an important control of stylolite morphology because clay minerals enhance the pressure solution process [37–41]. Other factors, such as burial depth and stress evolution of a basin [42–47], the diagenetic overprint [48,49] and the available pore fluids [9,44,50–52], can also play a key role in determining their formation.

Several models have been proposed to explain the mechanism controlling stylolite roughening [5,26,36,42,44,53]. However, there is still a lack of systematic geometrical

characterization of stylolites and how they relate to the sedimentary and diagenetic features of a wide variety of host rocks. Moreover, ref. [54] explained the complex geometry of stylolites as a result of the development of dissolution peaks and the mechanical properties at the interfaces between host rock and fluid. Stylolite thickness is typically affected by the heterogeneities in the original host rock. Indeed, ref. [1] noticed that the stylolite thickness is not constant along the entire length of the structure but generally decreases towards the tips of rough peaks. In this regard, ref. [55] suggested that the stylolite thickness/linearity relationship is constant, leading to the hypothesis that stylolites form at seed points and propagate laterally, undergoing dissolution at their flanks [56,57].

Stylolites with high amplitudes and wavelengths generally form closely spaced networks, sometimes anastomosing, in mud-dominated facies, while more widely spaced stylolites with low amplitude and low wavelength are more typical of grain-dominated rocks [20,23,30,41]. Moreover, poorly sorted facies tend to favour larger stylolite amplitudes and wavelengths [30]. Grain size and grain size distribution are also important due to the different solubility of the carbonate components, as well as their variable dissolution rates [58,59]. For example, the magnesium content of carbonate rock, together with the presence of certain skeletal components, can induce solubility variations in the rock [33], which affect stylolite formation. The aforementioned aspects highlight the importance of systematically characterizing the factors that control stylolite morphology to understand and predict their distribution and potential impact on fluid flow.

Despite the abundant literature on the relationship between stylolite length and thickness [55,60,61], a systematic quantitative database on the relationship between stylolite morphology, their geometrical parameters (linearity, spacing, thickness, insoluble material, connectivity, etc.) and the characteristics of their host rocks is still lacking. The works of [30,32] provided new insights into those relationships, but a more systematic quantification is needed. Therefore, this study aims to evaluate the geometrical parameters of stylolites in carbonate rocks to identify key controls on stylolite development and morphology. The specific objectives are (i) to characterize morphological parameters such as linearity, thickness, filling by insoluble material, spacing and connectivity in a variety of carbonate rocks with diverse rock textures and (ii) to establish relationships between such parameters and stylolite types according to Koehn et al.'s classification [29] and to depositional rock textures according to Dunham's classification scheme [62]. For this purpose, we used a large collection of samples collected from outcrops and ornamental stone sellers.

2. Materials and Methods

Stylolites were analyzed in 50 limestone samples from 30 locations in Europe, Africa and Asia (Table 1). Samples were collected in the field or purchased from ornamental rock sellers. Acquiring samples from rock sellers provides the opportunity to analyze a wide variety of stylolite morphologies in diverse limestone facies. However, the sample collection has the following limitations: (i) we tried to make thin sections at random parts of each sample, but it is possible that in some cases, the parts of the specimen with higher stylolite presence were unconsciously sampled; (ii) almost all the investigated stylolites are sedimentary; (iii) we do not have information about the burial depth at which each stylolite formed, since quantifying it would require the use of stylolite roughness inversion techniques [3,31,42–44], and this is beyond the scope of this study; and (iv) several samples show a transition between two rock textures (e.g., wackestone to packstone). In the latter case, a decision is made to classify the sample according to the rock texture in which the stylolite developed (Table 1).

Table 1. Summary of the analyzed samples showing age, origin by country, texture (sensu [62]) and main components. Note that age information is lacking for several samples. N/A means information is not available.

ID	Age	Location	Rock Texture	Main Grain Components
1	Cretaceous	Italy	Mudstone	Algal fragments, microforaminifera
2	Carboniferous?	Portugal	Mudstone	-
3	Triassic/Jurassic	Italy	Mudstone	Peloids, foraminifera
4	Cretaceous?	Spain	Wackestone	Algae fragments
5	N/A	Germany	Packstone	Peloids, intraclasts
6	Cretaceous	Belgium	Packstone	Lithoclasts
7	Miocene?	Spain	Wackestone	Sponge spicules
8	Eocene?	Italy	Packstone	Foraminifera, red algae
9	N/A	France	Wackestone	Crinoids, bioclasts
10	Eocene	Italy	Mudstone	Benthic foraminifera, ostracods
11	N/A	Spain?	Packstone	Foraminifera, red algae
12	Miocene	Italy	Packstone	Foraminifera, red algae, bryozoan
13	N/A	Turkey	Grainstone	Foraminifera, red algae
14	N/A	Spain	Wackestone	Foraminifera, bivalves
15	Cretaceous?	Spain	Wackestone	Foraminifera
16	Early Mesozoic	Egypt	Wackestone	Crinoids
17	N/A	Italy	Wackestone	Peloids, dolomite crystals
18	Jurassic	Italy	Mudstone	-
19	N/A	China	Mudstone	-
20	Cretaceous?	Pakistan	Packstone	Bivalve fragments
21	Triassic	Italy	Packstone	Bivalves, crinoids
22	N/A	Egypt	Packstone	Microforaminifera, bryozoans
23	Cretaceous	France	Wackestone	Nummulitids
24	Cretaceous?	Spain	Packstone	Orbitolinids
25	N/A	N/A	Mudstone	-
26	N/A	Italy	Mudstone	Calpionelle
27	N/A	Italy	Packstone	Calpionelle, ostracods
28	Cretaceous	Italy	Mudstone	Ostracods, foraminifera
29	N/A	Egypt	Wackestone	Bivalve fragments
30	N/A	Egypt	Wackestone	Bioclasts
31	N/A	France	Wackestone	Brachiopods
32	N/A	Greece	Packstone	Brachiopods
33	N/A	Italy	Grainstone	Crinoids
34	Lower Cretaceous	Italy	Wackestone	Dolomite crystals
35	N/A	Spain	Wackestone	Bioclasts
36	Eocene	Egypt	Packstone	Nummulitids
37	N/A	Turkey	Wackestone	Peloids, bryozoans and foraminifera
38	N/A	Morocco	Mudstone	Bryozoans

Table 1. *Cont.*

ID	Age	Location	Rock Texture	Main Grain Components
39	N/A	Morocco	Mudstone	Bryozoans
40	N/A	Turkey	Wackestone	Crinoids
41	Late Aptian	Spain	Grainstone	Orbitolinids, peloids, equinoderms
42	Late Aptian	Spain	Grainstone	Peloids, orbitolinids, equinoderms
43	Late Aptian	Spain	Grainstone	Peloids, echinoderms, miliolids
44	Late Aptian	Spain	Grainstone	Orbitolinids, peloids, echinoderms, red algae
45	Late Aptian	Spain	Grainstone	Orbitolinids, peloids, echinoderms, intraclasts
46	Aeolian-Bajocian	Spain	Grainstone	Oolites
47	Aeolian-Bajocian	Spain	Grainstone	Peloids, intraclasts
48	Aeolian-Bajocian	Spain	Grainstone	Peloids, coated grains
49	Late Aptian	Spain	Grainstone	Foraminifera, peloids, equinoderms

A standard thin section was made for each of the 50 samples and analyzed by optical microscopy. The petrographic analysis includes the characterization of the depositional limestone texture according to Dunham's scheme [62], diagenetic products and the stylolite types according to the scheme of Koehn et al. [29]. In addition, thin sections were scanned at high resolution (9600DPI), and several parameters were measured using vector image-processing software (Inkscape, V1.3) (stylolite linearity (length ratio), thickness, presence of insoluble material, spacing and connectivity) (Table 2). Other parameters, such as stylolite wavelength and amplitude, are not included in this paper. The reason is that much larger samples would be required to systematically measure wavelengths, while the amplitude trend is better evaluated at different scales, from the thin section to the outcrop scale, for instance.

Table 2. Summary of the stylolite parameters measured for each sample.

ID	Rock Texture	Stylolite Type	Stylolite Linearity			Filling with Insolubles (%)	Thickness (mm)	Spacing (mm)	Connectivity
			Upper Interface	Lower Interface	Average				
1	Mudstone	Seismogram pinning	0.26	N/A	0.26	16	0.57	11.51	SN
2	Mudstone	Suture and sharp peak	0.64	0.58	0.61	63	0.27	8.11	I
3	Mudstone	Suture and sharp peak	0.58	N/A	0.58	37	0.26	10.28	I
4	Wackestone	Suture and sharp peak	0.37	0.31	0.34	100	0.60	15.62	SN
5	Packstone	Suture and sharp peak	0.57	0.63	0.60	81	0.90	12.89	SN
6	Packstone	Simple wave-like	0.73	0.66	0.70	100	0.85	6.28	SN
7	Wackestone	Simple wave-like	0.90	0.71	0.80	100	0.15	4.77	SN
8	Packstone	Simple wave-like	0.72	0.65	0.69	23	0.29	14.35	I
9	Wackestone	Suture and sharp peak	0.44	0.51	0.47	79	0.16	8.44	I
10	Mudstone	Simple wave-like	0.71	0.74	0.73	98	1.05	30.47	SN
11	Packstone	Suture and sharp peak	0.59	N/A	0.59	0	0.17	4.30	SN
12	Packstone	Seismogram pinning	N/A	0.40	0.40	96	0.28	-	I
13	Grainstone	Seismogram pinning	0.46	0.66	0.56	98	1.35	9.94	SN
14	Wackestone	Suture and sharp peak	0.32	0.27	0.29	100	0.33	-	I
15	Wackestone	Simple wave-like	0.59	0.62	0.61	0	0.14	6.99	I
16	Wackestone	Simple wave-like	0.64	0.67	0.65	100	0.17	20.22	SN
17	Wackestone	Simple wave-like	0.70	0.70	0.70	100	0.48	10.05	SN
18	Mudstone	Simple wave-like	0.81	0.90	0.85	85	0.27	4.62	I
19	Mudstone	Seismogram pinning	0.46	0.37	0.41	75	0.28	11.18	SN
20	Packstone	Simple wave-like	0.85	0.83	0.84	0	0.57	22.89	I
21	Packstone	Rectangular layer	0.30	0.23	0.26	97	0.34	8.01	SN
22	Packstone	Seismogram pinning	0.32	0.36	0.34	100	0.79	3.96	LP
23	Wackestone	Suture and sharp peak	0.50	0.49	0.50	100	0.25	8.90	LP
24	Packstone	Suture and sharp peak	0.54	0.57	0.55	100	0.22	5.79	SN
25	Mudstone	Suture and sharp peak	0.51	0.51	0.51	87	0.20	10.24	SN
26	Mudstone	Seismogram pinning	0.52	N/A	0.52	100	0.19	6.90	SN
27	Packstone	Seismogram pinning	0.59	0.55	0.57	99	0.15	4.98	SN
28	Mudstone	Rectangular layer	0.34	0.27	0.30	96	0.56	6.65	LP
29	Wackestone	Suture and sharp peak	0.46	0.37	0.42	100	0.34	8.42	SN

Table 2. *Cont.*

ID	Rock Texture	Stylolite Type	Stylolite Linearity			Filling with Insolubles (%)	Thickness (mm)	Spacing (mm)	Connectivity
			Upper Interface	Lower Interface	Average				
30	Wackestone	Suture and sharp peak	0.33	0.27	0.30	62	0.40	4.44	I
31	Wackestone	Seismogram pinning	0.66	0.53	0.59	99	0.63	3.89	SN
32	Packstone	Suture and sharp peak	0.42	0.69	0.56	0	0.36	3.74	SN
33	Grainstone	Simple wave-like	0.76	0.75	0.75	0	0.67	-	I
34	Wackestone	Suture and sharp peak	0.51	0.60	0.55	100	0.63	7.95	SN
35	Wackestone	Rectangular layer	0.25	0.22	0.24	65	0.27	3.46	SN
36	Packstone	Suture and sharp peak	0.54	0.48	0.51	0	0.44	4.15	I
37	Wackestone	Suture and sharp peak	0.21	0.26	0.24	100	0.72	3.47	SN
38	Mudstone	Suture and sharp peak	0.66	0.74	0.70	82	1.31	11.07	SN
39	Mudstone	Suture and sharp peak	N/A	0.59	0.59	49	0.05	3.29	SN
40	Wackestone	Suture and sharp peak	0.61	0.62	0.61	62	0.95	4.81	I
41	Grainstone	Suture and sharp peak	0.68	0.66	0.67	8	0.20	17.34	I
42	Grainstone	Suture and sharp peak	0.43	0.41	0.42	29	0.05	10.49	I
43	Grainstone	Suture and sharp peak	0.69	0.68	0.69	99	0.12	9.06	I
44	Grainstone	Suture and sharp peak	0.60	0.54	0.57	41	0.13	12.15	I
45	Grainstone	Suture and sharp peak	0.58	0.71	0.65	99	0.34	4.68	I
46	Grainstone	Suture and sharp peak	0.43	0.41	0.42	97	0.10	14.4	I
47	Grainstone	Suture and sharp peak	0.45	0.48	0.46	79	0.22	8.56	SN
48	Grainstone	Suture and sharp peak	0.80	0.79	0.80	100	0.09	3.81	I
49	Grainstone	Simple wave-like	0.67	0.90	0.79	0	0.21	7.78	SN
50	Grainstone	Rectangular layer	0.79	0.99	0.89	98	0.22	5.89	SN

Note that for connectivity, "I" refers to isolated stylolites, "LP" to long-parallel stylolites and "SN" to stylolite networks. N/A means that these data could not be collected. In cases where there is only a linearity value for one of the interfaces, the average is just considered this value.

The stylolite linearity, also noted as the length ratio, results from dividing the straight length of the stylolite (i.e., the distance between stylolite endpoints in the thin section) by the total length (i.e., the distance measured along the stylolite trace) (Figure 2). The stylolite linearity was calculated to assess the relation between the stylolite roughness and their host rock textures, enabling the normalization of length measurements. The stylolite linearity varies from zero for infinitely rough stylolites to one for a perfectly straight stylolite. The linearity index was determined for the most representative and longest stylolites in each analyzed thin section. Length data were collected on both stylolite interfaces (upper and lower) (Figure 2). For very thin stylolites (6 out of 50 samples), we could only measure the length ratio on one stylolite interface, either the upper or lower.

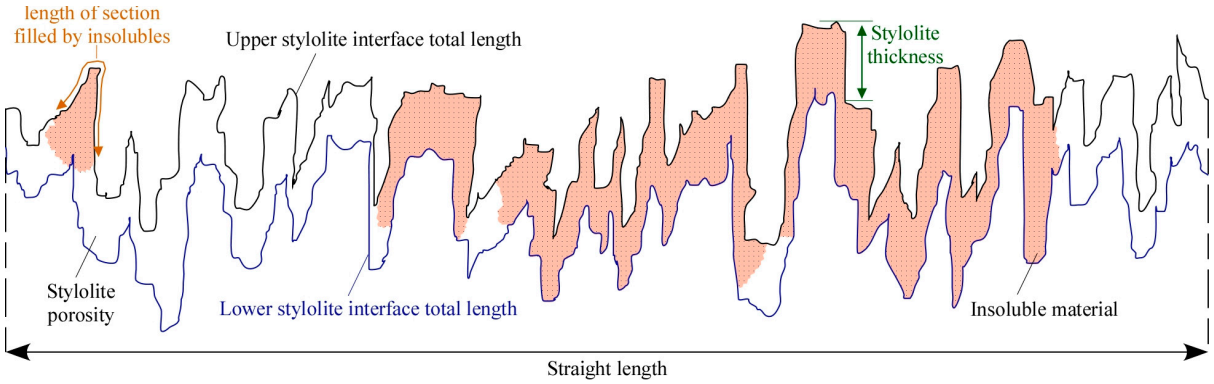

Figure 2. Sketch showing the stylolite measured parameters.

The stylolite thickness is defined as the distance between the lower and upper interfaces of the stylolite seam. It is never constant along the whole length of the stylolite and is generally larger at stylolite peak zones. The stylolite thickness was measured every 1 mm along a stylolite and then averaged for that stylolite (Figure 2). Sometimes, stylolites are very thin, and, in such cases, measuring their thickness can be challenging. However, the high resolution of thin section scans allows measuring very thin stylolites.

The stylolite spacing is the distance between two consecutive stylolites at the scale of observation (thin section in our case) and, therefore, cannot be considered a fully direct representation of the real distribution of stylolites in the field since this spacing can vary horizontally. The scanline to measure stylolite spacing was positioned to intersect the greatest possible number of stylolites present in a specific thin section (Figure 2). It is important to consider that we worked on small areas (standard thin sections, with a size of ca. 5 × 3 cm.) compared to previous similar analyses [30].

Stylolite connectivity defines the link between one stylolite and its neighbours (Figure 1b). The stylolite connectivity classification scheme considers three types of connectivity, according to [9]: (i) isolated (I), when there is only one stylolite in the sampling area (i.e., thin section); (ii) long-parallel (LP), when there is more than one stylolite but they do not intersect; and (iii) anastomosing stylolite network (SN), when there are several stylolites that are connected or intersect each other (Figure 2). The small sampling areas corresponding to a standard thin section area do not allow for carrying out a topological analysis.

The insoluble material length ratio quantifies the accumulation of residual or undissolved material along the stylolite surface. This parameter is calculated by measuring the sum of lengths of stylolite sections that are filled with insoluble material divided by the total stylolite length (filled or not with insolubles). The parameter is calculated as the average of the result of the two stylolite interfaces, i.e., upper and lower), following its trace (Figure 2). The final value is expressed as a percentage of the stylolite length filled with residue. It is important to note that part of the insoluble material can be unintentionally removed during thin section preparation, and thus, the results should be considered as a minimum value. The value ranges from one, meaning a stylolite that continuously contains insoluble material along its full length, to zero for a stylolite that does not contain insoluble material (i.e., is an open space).

All the investigated parameters were organized and plotted in relation to the Dunham host rock texture [62] and stylolite types of Koehn et al. [29]. Sometimes, the stylolite shape, especially for rectangular and seismogram types, is difficult to assign to a single category.

3. Results

3.1. Host Rock Texture and Components

The most important characteristics of the host rock textures in investigated samples are described according to Dunham's classification [62] (Figure 3). In terms of the carbonate rock texture, wackestones are the most abundant among the studied samples (30%), while mudstones (22%), packstones (24%) and grainstones (24%) are nearly equally represented (Table 1). Several thin sections show local texture transitions (i.e., from mudstone to wackestones, or wackestone to packstone) making it sometimes hard to associate each sample, and hence its stylolites, with a single rock texture.

Mudstone samples range in age between Jurassic and Eocene, although most of them are from Lower to Upper Cretaceous outcrops (Table 1, Figure 3a,b). The most common skeletal components, often found in fragments and chaotically oriented, are red algae, calpionelle and foraminifera, while bryozoan and crinoids are occasionally represented. Skeletal components are rarely larger than 2 mm. Few mudstones lack skeletal components but contain intraclasts and calcite cement. Wackestones vary from Jurassic to Miocene in age and contain skeletal components, mostly crinoids and foraminifera, generally as fragments (Table 1, Figure 3c,d). Less frequently, wackestones also contain bivalves and bryozoans. Packstones range in age from Triassic to Miocene except for a Devonian sample (Table 1, Figure 3e,f). Foraminifera, red algae, bryozoa and bivalves are the most abundant skeletal components in such texture. Two samples show calpionelle and ostracods. Nummulites are recognized in one Eocene rock sample. Grainstones range in age from Middle Jurassic to

Lower Cretaceous (Table 1, Figure 3g,h). The most abundant components in this lithology are orbitolinids, peloids, echinoderms, red algae and, especially, intraclasts.

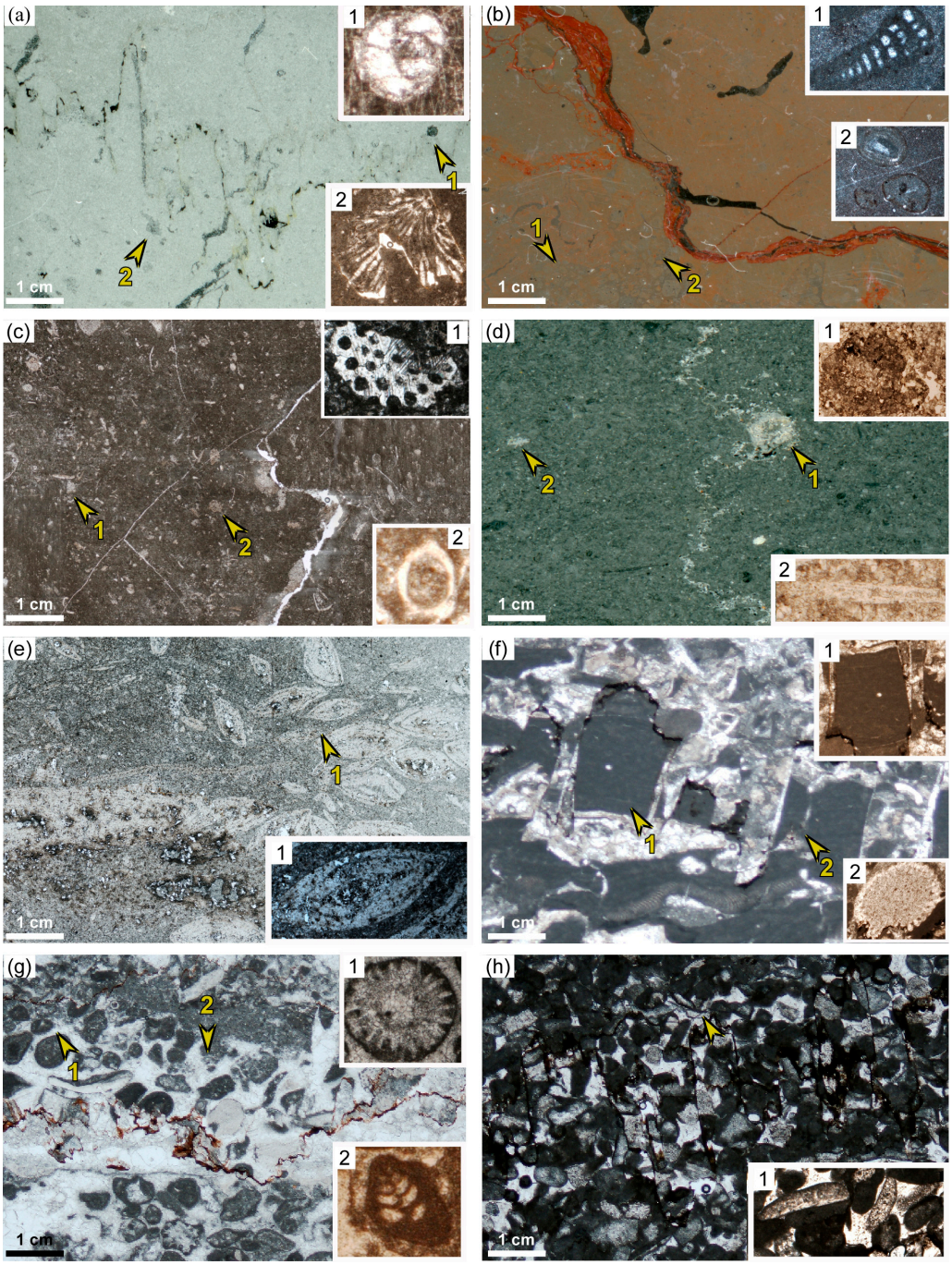

Figure 3. Photomicrographs showing examples of rock textures in several carbonate facies. (**a**) Mudstone with foraminifera (1) and bryozoans (2). (**b**) Mudstone with benthic foraminifera (1) and oncoids (2) inside a Neptunian dyke. (**c**) Wackestone with bryozoans (1) and calcispheres (2). (**d**) Wackestone with intraclasts (1) and algae (2). (**e**) Packstone with nummulites (1). (**f**) Packstone with intraclasts of stromatoporoidea (1) and echinoidea (2). (**g**) Packstone with echinoidea (1) and foraminifera (2). (**h**) Grainstone with elongated fragments of brachiopods (1).

3.2. Stylolite Types

Investigated stylolites (Figure 4) are described according to the scheme of Koehn et al. [29], and their abundance is quantified in relation to the corresponding carbonate host rock texture (Figure 5). The four stylolite types are represented in the dataset as follows: rectan-

gular layer type (8%), seismogram pinning type (18%), suture and sharp peak type (52%) and simple wave-like type (22%). The rectangular layer type is scarce, although it has been identified in all the rock textures.

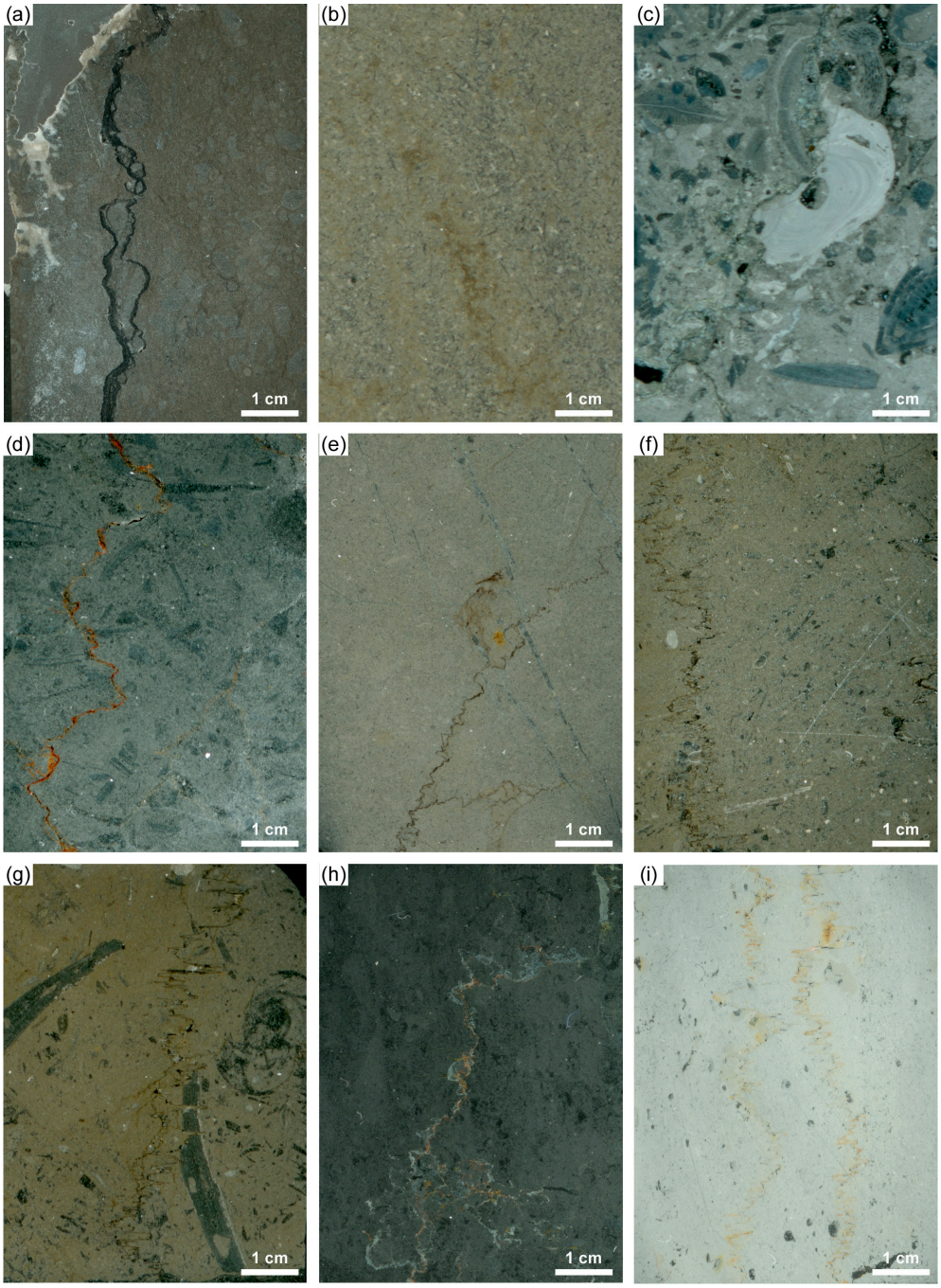

Figure 4. Photomicrographs showing examples of stylolite types. (**a**) Wave-like type in packstone (Tables 1 and 2, sample 9). (**b**) Thin wave-like stylolite in wackestone (Tables 1 and 2, sample 7). Note how the stylolite trace is recognizable due to the presence of the dark, insoluble material. (**c**) Wave-like stylolite in packstone (Tables 1 and 2, sample 10). (**d**) Suture and sharp peak-type stylolite with accumulated insoluble material (Tables 1 and 2, sample 17). (**e**) Seismogram pinning-type stylolite in a wackestone (Tables 1 and 2, sample 29). (**f**) Rectangular layer-type stylolite in wackestone (Tables 1 and 2, sample 38). (**g**) Rectangular layer type in packstone (Tables 1 and 2, sample 24). (**h**) Suture and sharp peak stylolite in wackestone with yellow insoluble material filling (Tables 1 and 2, sample 6). (**i**) Rectangular layer-type stylolite in mudstone (Tables 1 and 2, sample 31).

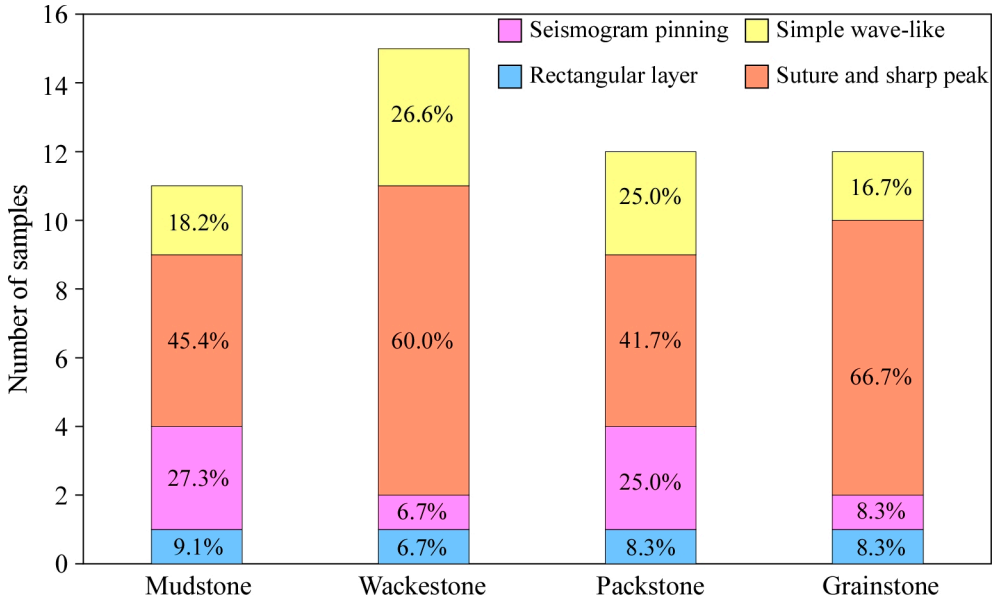

Figure 5. Distribution of stylolite types (according to the scheme of [29]) *versus* rock texture (according to the Dunham scheme [62]).

The most abundant stylolite type in mudstones is the suture and sharp peak type (45.5%), followed by the seismogram pinning (27.3%) and simple wave-like types (18.2%) (Figure 5). In wackestones, which is the dominant rock texture in the dataset, the most common stylolite type is the suture and sharp peak type (60.0%), followed by the wave-like type (26.7%). Moreover, there is one sample with seismogram pinning (6.7%) and one rectangular layer (6.7%) of stylolite types observed in this rock texture. Suture and sharp peak-type stylolites are dominant in packstones (41.7%), followed by seismogram pinning (25.0%) and wave-like types (25.0%). There is one sample with rectangular layer-type stylolites (representing 8.3% of the population) in this rock texture. Grainstones show the same trend as packstones in terms of abundance of stylolite types: suture and sharp peak are the dominant type (66.7%), followed by wave-like type (16.7%). Rectangular layer and seismogram pinning-type stylolites represent 8.3% of the dataset each. The stylolites hosted in grainstones are thinner compared to other rock textures. Stylolites often follow grain contacts in grain-dominated textures.

3.3. Stylolite Morphological Properties

3.3.1. Stylolite Linearity

The linearity of stylolites provides information on their sinuosity and therefore how rough or straight a stylolite is (Figure 6). Linearity results show that the highest stylolite linearity is observed in grainstones (i.e., more linear, with a median of 0.67), followed by mudstones (median 0.58) and packstones (median 0.57), while wackestones show the lowest ratio (i.e., more contorted stylolites with a median of 0.51) (Figure 6a). In terms of the stylolite morphology, wave-like-type stylolites show the highest linearity (with a median of 0.72) (Figure 6b). They are abundant in facies with wackestone and packstone textures (Figure 5). The other types of stylolites present linearity values that decrease from the suture and sharp peak (median of 0.54) to seismogram pinning (median of 0.46) to the rectangular layer type (the most contorted with a median of 0.28).

Regarding stylolite types, there is an increasing trend from the rectangular layer stylolite type (most contorted) to the wave-like stylolite type (more linear) (Figure 6b). In this regard, the linearity value increases around 10% from the rectangular layer to seismogram pinning, suture and sharp peak and, finally, to the wave-like stylolite types.

The linearity is slightly different when it is measured on the two interfaces (upper and lower) of a stylolite but commonly presents the same trend for both. The difference in linearity between both interfaces is very low when plotted against rock texture or stylolite type (Figure 6). There is a slightly higher difference between the linearity of the upper and lower interfaces of rectangular layer-type stylolites, although the population in Figure 6b (blue boxes) is clearly influenced by an outlier.

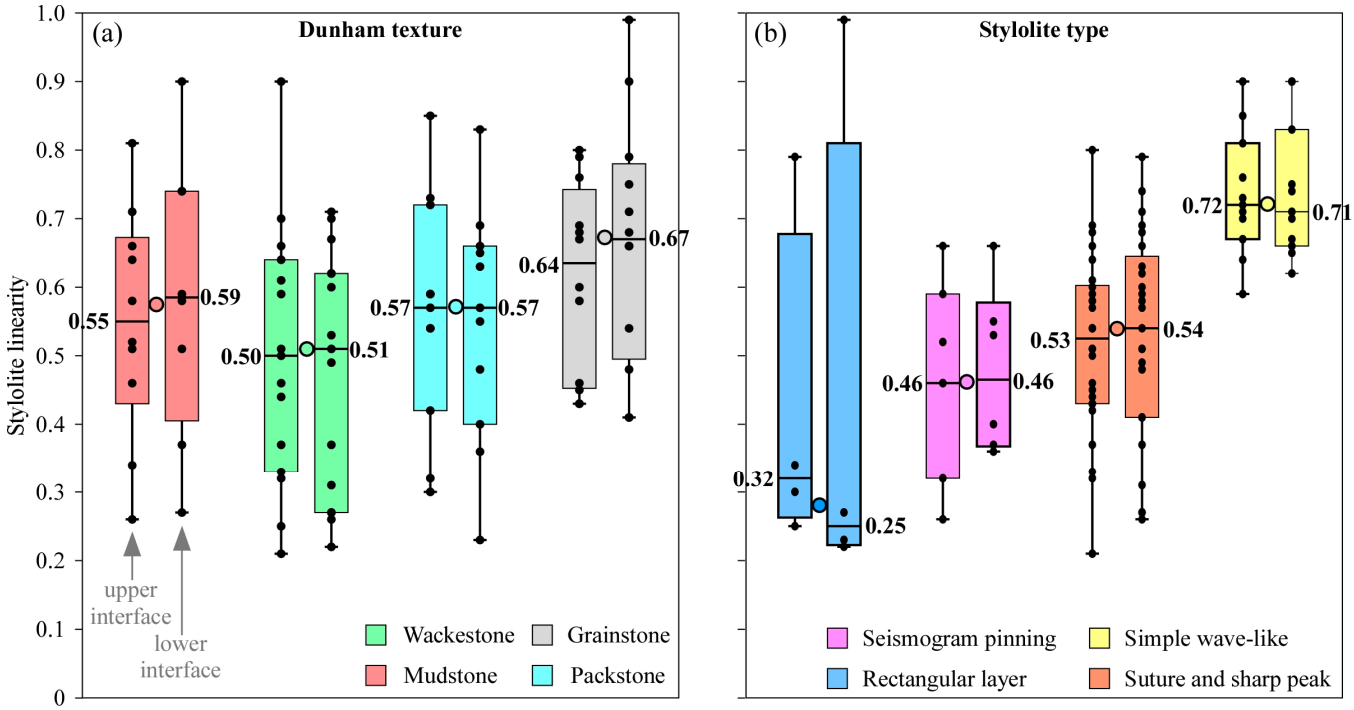

Figure 6. Box and jitter plots showing the stylolite linearity (ratio of total length and straight length) for Dunham rock textures (**a**) and stylolite types (**b**). Each coloured box marks the 25 and 75 percent quartiles for each dataset, which correspond to the upper and lower interfaces of stylolites for each rock texture or stylolite type. The median of each dataset is indicated with a horizontal line in the box, and the corresponding median value is also provided. The black vertical lines show the minimal and maximal values of each dataset, while each black dot represents an individual measurement. The circles filled with the corresponding colour indicate the median of the population. For Dunham textures, they are 0.58 for mudstones, 0.51 for wackestones, 0.57 for packstones and 0.67 for grainstones, while for stylolite types, they are 0.28 for rectangular layer, 0.46 for seismogram pinning, 0.54 for suture and sharp peak and 0.72 for simple wave-like stylolite types.

3.3.2. Stylolite Thickness

The stylolite thickness analysis (i.e., the distance between the lower and upper stylolitic interfaces) reveals that stylolites developed in grainstones tend to be thinner, with a median of 0.21 mm, especially considering that there is a high outlier. Stylolites hosted in mudstones are slightly thicker on average (median of 0.27 mm) but with a wide variation. Stylolites in wackestones and packstones are the thickest, with a median of 0.34 mm and 0.35 mm, respectively (Figure 7a). In terms of stylolite types, the highest thickness is measured on the seismogram pinning stylolites (median of 0.43 mm), while the lowest one corresponds to suture and sharp peak stylolite type (median of 0.26 mm) (Figure 7b). Rectangular layer type and simple wave-like-type stylolites show very similar thickness values (0.31 and 0.29 mm, respectively). The data variability is very high for all types except for the rectangular layer-type stylolites, which tend to show more consistent values.

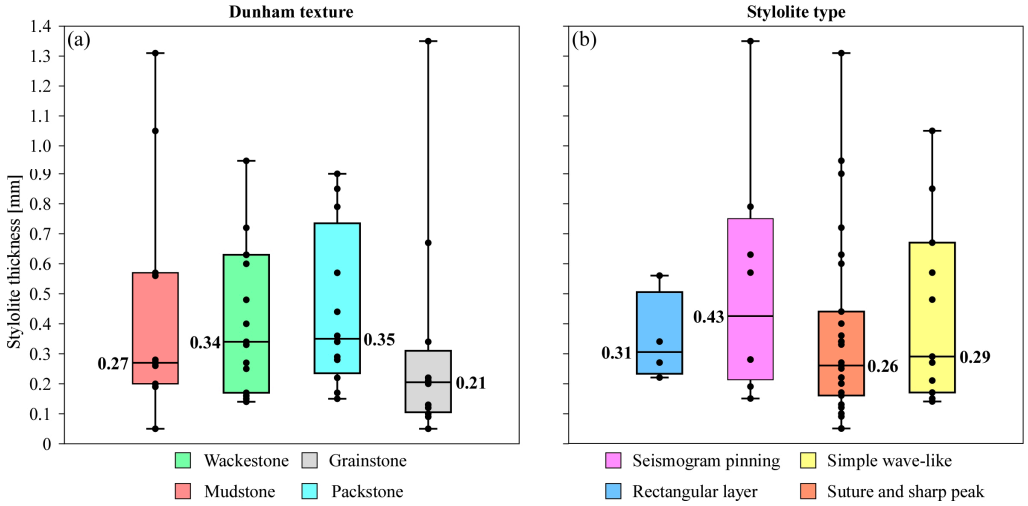

Figure 7. Stylolite thickness for Dunham rock textures (**a**) and stylolite types (**b**). Each coloured box marks the 25 and 75 percent quartiles for each dataset, which correspond to each rock texture or stylolite type. The median of each dataset is indicated with a horizontal line in the box, and the corresponding median value is also provided. The black vertical lines show the minimal and maximal values of each dataset, while each black dot represents an individual measurement.

3.3.3. Insoluble Material Along Stylolites

The highest amount of insoluble material, which is expressed as the percentage calculated from the ratio between the stylolite length filled with insoluble material and the total stylolite length, appears in stylolites hosted in wackestones (median 100%), while mudstones show the lowest value (median 82%) (Figure 8a). Packstones and grainstones show the same amount of filling by insoluble material (median 88%). In terms of stylolite type, a higher amount of insoluble material is observed for seismogram pinning-type stylolites (median 98%), followed by the rectangular layer type (median 96%). Simple wave-like and suture and sharp peak-type stylolites appear to contain slightly fewer parts filled by insoluble material along them (median of 81% and 85%, respectively) (Figure 8b).

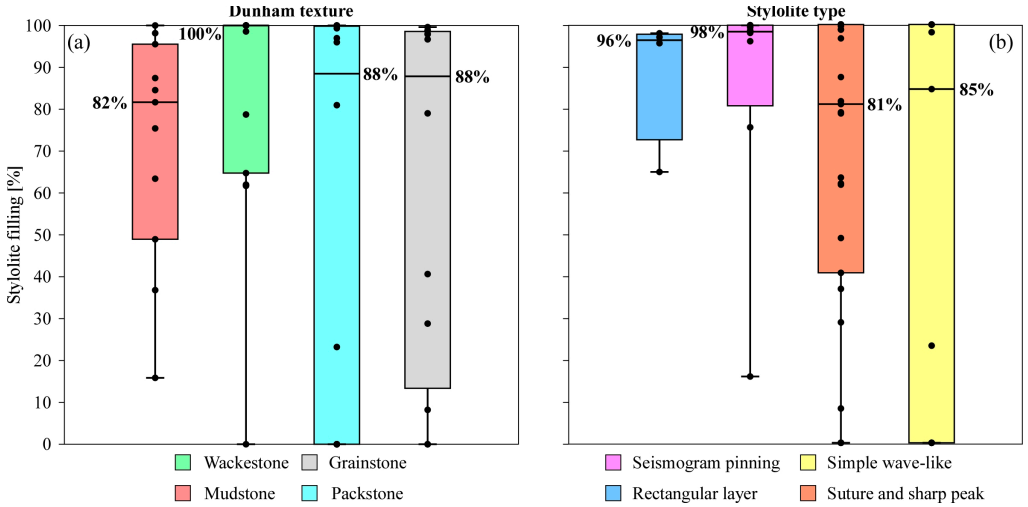

Figure 8. Plots showing the percentage of filling with insolubles, calculated from the ratio of stylolite length filled with insoluble material over the total stylolite length for Dunham rock texture (**a**) and stylolite type (**b**). Each coloured box marks the 25 and 75 percent quartiles for each dataset, which correspond to each rock texture or stylolite type. The median of each dataset is indicated with a horizontal line in the box, and the corresponding median value is also provided. The black vertical lines show the minimal and maximal values of each dataset, while each black dot represents an individual measurement.

The stylolite thickness and length ratio of insoluble material do not correlate well since there is a high variability of values for the stylolite filling with insolubles. The highest thickness and length ratio of insoluble material is observed for seismogram pinning-type stylolites, while rectangular layer-type stylolites almost have the same thickness on average as simple wave-like stylolites, but the filling with insoluble material is significantly higher for the first type compared to the simple wave-like stylolites. Suture and sharp peak stylolites feature the lowest thickness and also the lowest percentage of filled length (Figures 7 and 8).

3.3.4. Stylolite Spacing

The stylolite spacing represents the density of stylolites for each sample at the scale of the thin section. The maximum spacing appears in mudstones (with a median of 10.24 mm) followed by grainstones (9.06 mm) (Figure 9). Wackestones present a spacing of 7.74 mm, while packstones show the lowest spacing (5.79 mm) and thus the higher density of stylolite of all textures (Figure 9a). In terms of stylolite type, rectangular layer-type stylolites show the lowest spacing (with a median of 6.27 mm) and thus the highest stylolite density, while simple wave-like stylolites are the ones with higher spacing (median of 8.92 mm). The spacing of seismogram pinning and suture and sharp peak stylolites is in between that of the other types (median of 6.90 and 8.43, respectively) (Figure 9b).

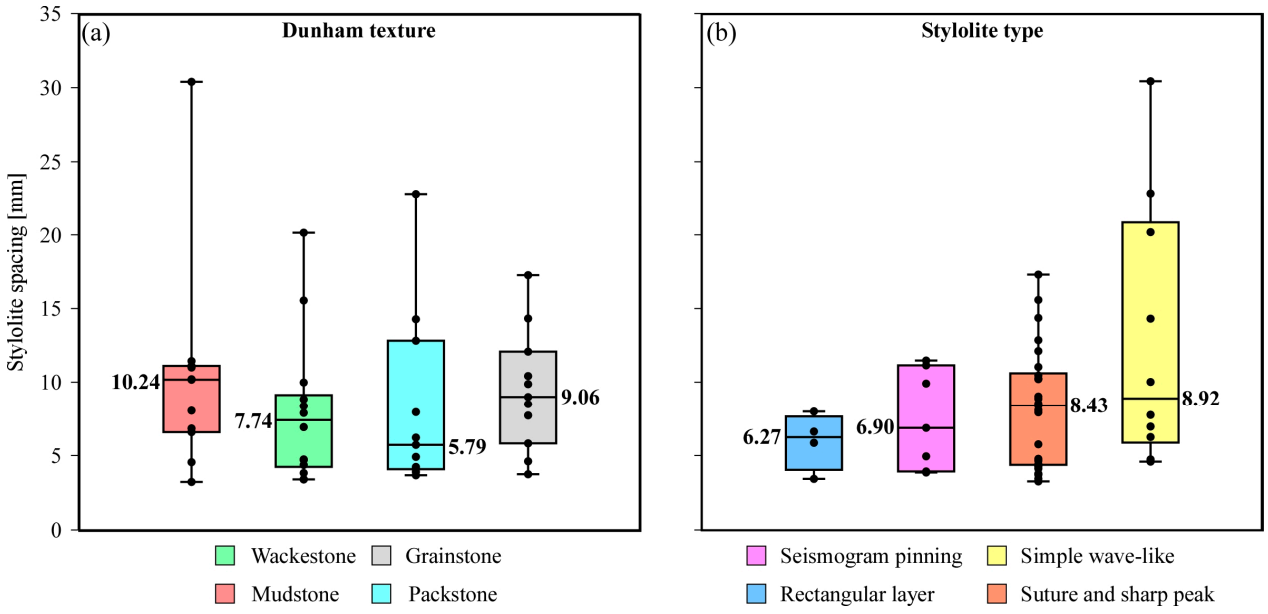

Figure 9. Plots showing the maximum stylolite spacing, measured perpendicular to each stylolite set, for Dunham rock texture (**a**) and stylolite type (**b**). Each coloured box marks the 25 and 75 percent quartiles for each dataset, which correspond to each rock texture or stylolite type. The median of each dataset is indicated with a horizontal line in the box, and the corresponding median value is also provided. The black vertical lines show the minimal and maximal values of each dataset, while each black dot represents an individual measurement.

3.3.5. Stylolite Connectivity

The analysis of stylolite connectivity is influenced by the small area of observation corresponding to a thin section. However, this analysis can still provide useful observations. The results show that the long parallel stylolite distribution type is very scarce for all the samples analyzed, regardless of stylolite type and limestone texture (Figure 10). Regarding rock textures, stylolite networks are more abundant in wackestones, being the same in packstones and mudstones, while they are quite scarce in grainstones (Figure 10a). By contrast,

isolated stylolites (i.e., not connected) are well represented in mudstones, wackestones and packstones and are abundant in the case of grainstone textures. Stylolites appear mostly isolated in grainstones, followed by mudstones and wackestones (Figure 10). Stylolite networks are more abundant in wackestones and packstones, especially those of the suture and sharp peak type, and in mudstones with seismogram pinning and suture and sharp peak types.

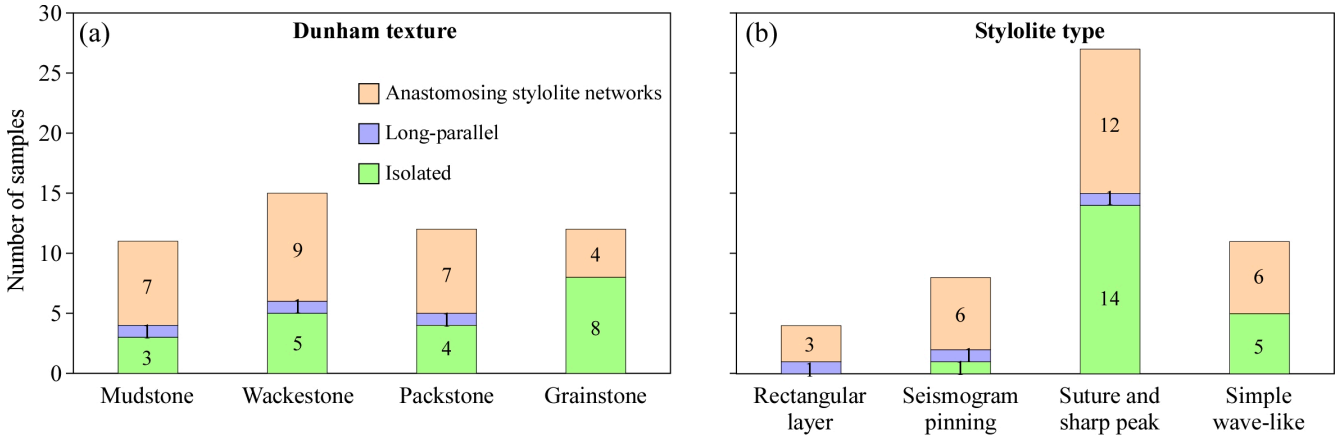

Figure 10. Distribution of stylolite connectivity (according to the scheme of [9]) *versus* Dunham rock texture (**a**) and stylolite type (**b**). The number of measurements is indicated within the box of each category.

Samples with simple wave-like stylolites or grainstone textures do not feature long parallel stylolites. Isolated stylolites and anastomosing stylolite networks are also scarce in samples with rectangular layer-type stylolites but increase in samples with seismogram pinning and simple wave-like types, especially in those with suture and sharp-type stylolites (Figure 10b). Long parallel stylolites are not well represented in our dataset. They are found in just three samples.

4. Discussion

4.1. Rock Textural Controls on Stylolite Types and Their Linearity

The analysis of stylolite abundance shows that the four stylolite types appear with variable abundance in all carbonate textures (Tables 1 and 2). Suture and sharp peaks are the most abundant stylolite types in the studied dataset (Figure 5), followed by the simple wave-like type. Moreover, suture and sharp peak stylolites are especially dominant in wackestones and grainstones. Our results are partially in agreement with those of [30], who reported a higher abundance of suture and sharp peak-type stylolites in grain-supported textures (packstones) compared to mud-supported ones. The analyzed datasets reveal that simple wave-like stylolites are more abundant in wackestones and packstones (Figure 5). This disagrees with the findings of [32], who reported a higher abundance of simple wave-like types in mudstones. However, the samples of [32] are from cap rocks of ultra-deep carbonate reservoirs, and the burial history may have also played a significant role in the resulting morphologies. Humprey et al. [30] observed that simple wave-like-type stylolites, and occasionally also rectangular layer-type ones, are abundant in grain-dominated textures. The disagreement between their and our dataset is partly attributed to the presence of transitional textures between mud- and grain-supported textures, but also by the scale of observation, as the dataset presented here is based on thin sections, and that of [30] is based on outcrop data.

The results indicate a slight increase in stylolite linearity from those hosted in mud-supported textures towards cases of grain-supported textures, suggesting that rock texture partially controls stylolite contortion (Figure 6a). However, there is a weak correlation between Dunham rock texture and stylolite morphology, as revealed by the very large range of linearity values for all the rock textures (Figure 6a). This can be potentially related to the variable presence of pinning particles, variable grain size and grain size distribution, and amount of micrite and clay content. Sometimes, the presence of larger grains embedded in a matrix, such as bioclasts in a wackestone, results in higher contortion. Other studies have reported similar stylolite types for different rock textures [30].

The difference in linearity measured for both (upper and lower) interfaces of stylolites is generally very low, except for the samples developed in mudstone and grainstone textures, which tend to show some divergence in that regard (Figure 6a). This is probably associated with a different growth rate of the stylolite at each interface, likely related to pinning particles or to the relative solubility of components at each stylolite side [3]. Local stress changes can also produce slight changes in stylolite morphology on both sides of the stylolite. The presence of clays is considered a key factor for stylolitization in fine-grained rocks because they enhance the diffusion of dissolved host rock [38,63,64] due to differences in electrochemical potential between these minerals and other rock components [40,58,65].

The sample analysis reveals that stylolite linearity increases from the rectangular layer towards the simple wave-like stylolite types (Figure 6b). This trend is in accordance with the growth mechanisms of the different types of stylolites reported by [29], which results in higher and lower peaks for the rectangular layer and seismogram pinning types compared to the other types. Conversely, the results denote a quite homogeneous distribution of linearity for the seismogram pinning, suture and sharp peak and simple wave-like types in mudstones and wackestones. The trend also indicates that rectangular layer and seismogram pinning stylolites are strongly influenced by local processes and pinning particles, whereas simple wave-like stylolites display more uniform growth patterns [29].

4.2. Rock Textural Controls on Stylolite Thickness and Insoluble Material

The stylolite thickness could be envisaged as the space originally occupied by insoluble material. Thus, higher thicknesses would imply a higher content of insoluble material. Considering the different limestone depositional textures, the results show a progressive increase in stylolite thickness from mudstones to wackestones and packstones (Figure 7a). However, grainstones yield significantly lower values compared to them. This suggests that depositional textures control, at least in part, stylolite thickness. However, packstone textures, with lower micrite and likely clay content than wackestones and mudstones, present, on average, a slightly higher stylolite thickness. The lower values and high dispersion of thickness data can also be attributed to local variations in grain size distribution that cause grain pinning [29,58] and to a variable number of clays [30]. Considering the different stylolite types, the results show a higher ratio of insoluble material in seismogram pinning-type stylolites hosted in packstones compared to the other stylolite types and rock textures (Figure 7b).

The distribution of insoluble material like clays and oxides along stylolites in limestones [18,27,53] and/or sulphides and oxides in sandstones [15,66] is likely related to porosity and solubility variations along the stylolitic surface [35,64,67]. There is generally a positive correlation between the distribution of insoluble material and the amount of dissolution [2,15]. According to [41], porosity is higher in grain-dominated textures (packstones and grainstones) than in mud-dominated facies (mudstones and wackestones). The variation in the porosity index is likely associated with remobilization by fluids circulating through the stylolite [50,68,69] or with heterogeneity in the mechanical and dissolution

properties of the insoluble material [70]. In this regard, SEM analyses suggest that the flow of fluids affects an area wider than just the stylolitic surface [70,71]. Contrary to macro-porosity, numerical modelling demonstrated that the nano-scale porosity may remain unchanged even if the rest of the pores clog up due to the high curvature of the small-scale pores [72,73].

Based on porosity and permeability tests, ref. [74] concluded that stylolites in carbonate cap rocks produce more complex pore networks compared to stylolite-free ones with a significant increase in permeability anisotropy [75]. Additionally, the chemical composition of the grains can influence the solubility and the growth of the stylolite, being Mg one of the key elements in terms of such properties [33]. Therefore, the Mg content of skeletal grains can potentially define the range of grain dissolution [76]. Stylolite porosity is not quantified in the present study since additional porosity is often generated while making the thin section when the powder used for polishing removes material from the stylolite seam.

Despite clays, iron oxides and sulphides have been suggested to enhance dissolution and stylolitization [15,18,27,53,66], their exact role is not fully understood. Several hypotheses have been proposed, including variations in chemical reactions due to changes in pH [77], enhancement of kinetic reactions due to the contact between calcite and insoluble material [38–40,65,78], and due to soft inclusions that concentrate stress [79]. In this regard, clay minerals have been identified as enhancers of stylolite roughening [20,33,41]. The results do not show a clear trend in terms of the distribution of insoluble material with respect to the host rock texture. Stylolites developed in wackestones exhibit the highest amount of insolubles compared to those developed in mudstones, packstones and grainstones.

The results presented here indicate that the amount of insoluble material is higher for rectangular layer and seismogram pinning-type stylolites, which are abundant in mudstones and packstones, as stylolite linearity increases (Figures 5 and 8). This behaviour has two main implications: (i) in the most non-linear stylolites, such as those of the rectangular layer and seismogram pinning types, insoluble material can particularly be concentrated in certain areas of higher stress [29,58]; and (ii) the pressure solution that determines the type of stylolite is also responsible for the accumulation of insoluble material along their surfaces. Therefore, in well-sorted rocks, there is a certain pressure homogeneity, which likely results in a more homogeneous distribution of insoluble material along the stylolitic surface. On the other hand, in cases in which pressure solution is strongly influenced by the presence of large grains, even with good sorting, or when grains have different solubility, the insoluble material will accumulate only in certain areas, leading to lower values of the ratio of insolubles. However, there are situations in which insolubles concentrate in relatively homogeneous and fine rocks [80]. The accumulation of insoluble material is positively, but weakly, correlated with stylolite thickness (Figure 11). For example, seismogram pinning stylolites tend to be thicker, and this is attributed to significant amounts of insoluble material, which reflect higher levels of dissolution and stress concentration. The distribution of insoluble material has a direct effect on the sealing capacity of the different types of stylolites [29,32,80]. In particular, rectangular layer-type stylolites can be more prone to act as pathways for fluids along their teeth [80], while seismogram pinning-type stylolites preferentially represent barriers, sutures and sharp peaks show an intermediate sealing capacity depending on the amount of insoluble material [32], and wave-like type would preferentially act as effective barriers for fluids [13,23,30]. Further work to quantify the amount of insoluble material in different rock types is suggested, although it is out of the scope of the present study.

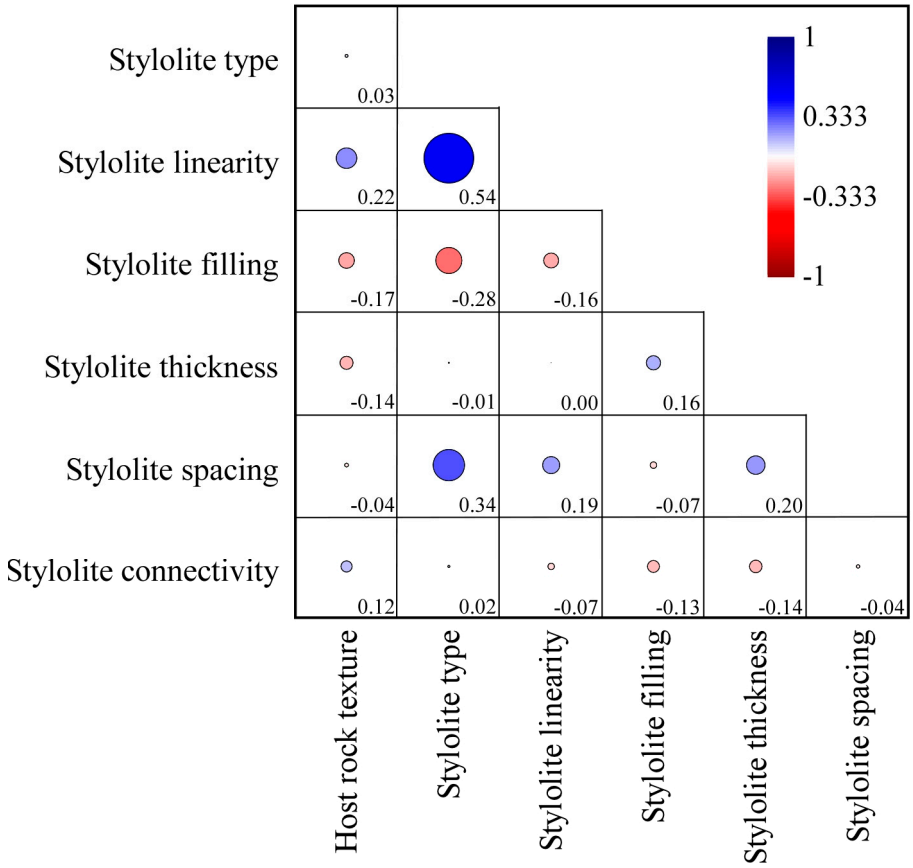

Figure 11. Correlation matrix showing the linear r (Pearson) correlation coefficient between stylolite and host rock measured parameters. The Pearson correlation coefficients range between −1 and +1, indicating negative and positive correlations, respectively, while a value of zero means no correlation. The value of the Pearson correlation coefficient is shown in the corresponding cell. The circle size ranges between 0 (no correlation) and −1 or +1 (maximum negative or positive correlation).

4.3. Rock Textural Controls on Stylolite Spacing

The stylolite spacing distribution is an important parameter to evaluate the dissolution of a sedimentary succession during burial. However, it should be noted that the stylolite spacing analysis presented here is performed at the thin section scale (Figure 9). According to Zeeb et al. [81], the spacing measurements are influenced by the resolution of the sample, which can lead to sampling bias. Therefore, in the case of small areas of observation like in this study (i.e., thin section) some stylolites may not be identified, which can probably lead to limitations in the estimation of spacing measurements.

Stylolite linearity and spacing show a very weak positive correlation (Figure 11). More contorted stylolites, such as those of the rectangular layer type, tend to form in localized high-stress areas with concentrated dissolution, allowing them to develop closer together. In contrast, more linear stylolites, like those of the simple wave-like type, would form under a more uniform stress distribution and dissolution, resulting in greater spacing between them. More linear stylolites (as those of the wave-like type), in principle, occupy lower volume in the rock and thus would tend to appear more widely spaced. Finally, the results indicate that stylolites developed in mudstones and grainstones are more widely spaced than those in wackestones and packstones (Figure 9), suggesting that heterogeneity in grain size, grain composition and sorting have an important role in controlling the formation of stylolites [26,30]. By contrast, ref. [53] concluded that stylolites are randomly spaced in the field.

Previous studies suggest that grain size and grain size distribution are key factors influencing stylolite spacing [42]. Rocks with larger and more uniformly distributed grains would tend to have wider stylolite spacing. Additionally, ref. [18,29] highlight that stress distribution during chemical compaction plays a critical role in a way that rocks with more homogeneous textures, such as grainstones, exhibit more evenly distributed stress, leading to greater spacing between stylolites. While stylolite spacing is discussed in relation to different rock textures, a more thorough analysis would be required to understand how local variations in grain size and porosity influence stylolite spacing.

4.4. Rock Textural Controls on Stylolite Connectivity

Stylolites can appear either isolated [56] or grouped forming networks [9]. The latter authors classified stylolite connectivity in several categories, with stylolites being isolated, long parallel or forming anastomosing networks (when they intersect). The formation of long-parallel stylolites has been related to the presence of strain energy on free faces of grains [82,83], clay [84], grain size heterogeneity [34] and continuous bedding planes that roughen by dissolution [5,29,35,44]. Moreover, the formation of long-parallel stylolites is commonly facilitated by the presence of large fossils that can enhance their formation [30]. Therefore, large fossils and grain size heterogeneity variations at different scales likely enhance the formation of stylolites with a long-parallel distribution [29]. In our dataset, long-parallel stylolites appear in one sample for each rock texture (Figure 10a), except for grainstones, and for each stylolite type except for wave-like ones (Figure 10b). The results indicate that anastomosing stylolite networks are the most abundant arrangement type, followed by isolated stylolites (Figure 10a). This indicates stylolites tend to arrange in networks rather than being isolated structures, as also reported from field studies [9,23,30]. Anastomosing stylolite networks are dominant in samples with suture and sharp peak-type stylolites, followed by wave-like types in mudstones, packstones and grainstones. Stylolite networks are more prevalent in textures with heterogeneous grain sizes, such as wackestones and packstones, probably due to local variations in grain size and solubility (related to grain composition). Such systems present appropriate conditions for stylolite connection and intersection. This agrees with [61], who concluded that stylolite networks are more abundant in mud-dominated facies. However, the amount of stylolite intersections in this study is remarkable, revealing that even with a small scale of observation, stylolite intersections can be traced.

4.5. Correlation Analysis of Stylolite and Host Rock Parameters

A linear correlation analysis between the parameters utilized was carried out to investigate their relationship with the carbonate depositional texture and stylolite types (Figure 11). The Pearson coefficients of the correlation matrix vary between -1 and 1. For the correlation calculation, we assigned the following values to the host rock texture: 1-mudstone, 2-wackestone, 3-packstone and 4-grainstone, and to the stylolite types: 1-rectangular layer, 2-seismogram pinning, 3-suture and sharp peak and 4-wave-like. The stylolite average linearity shows a good correlation with the stylolite type, meaning that suture and sharp peak and wave-like stylolites are less contorted than rectangular layer and seismogram pinning stylolites. The stylolite average linearity also correlates with the host rock depositional texture. A comparison with Figure 6 shows that stylolites progressively become slightly more linear when hosted in textures from wackestone to packstone to grainstone. However, those hosted in mudstones present a similar linearity as those in packstones. Therefore, this positive correlation does not always apply. Stylolite linearity shows a slightly good correlation with stylolite spacing, while it negatively correlates with stylolite filling by insoluble material. Stylolite thickness and filling by insoluble material

show a positive correlation, supporting the idea that the accumulation of material along the stylolitic surface increases as the stylolite grows. A negative correlation is observed between stylolite filling by insoluble material and rock texture. A comparison of this observation with Figure 8a reveals that this negative correlation is likely a consequence of the high variability in insoluble material filling in muddier host rock textures, which tend to show a slightly more heterogeneous behaviour in terms of insoluble stylolite filling than stylolites hosted in rocks with more grainy textures.

5. Conclusions

This contribution presents a study of stylolites in a set of carbonate rocks of diverse origins and types, specifically addressing the relationship between the stylolite morphological parameters and the depositional texture and type of stylolite. The results have resulted in the following conclusions:

Stylolite linearity progressively increases from a rectangular layer to seismogram pinning, to suture and sharp peak and to simple wave-like-type stylolites. Stylolite linearity is relatively similar for all host rock textures, although there is a trend for stylolites hosted in grainier host rocks to be slightly more linear.

Stylolite thickness increases from mudstones to wackestones and progressively reduces towards grainstones so that the rock textural control on stylolite thickness is unclear. Additionally, there is no clear distribution of stylolite thickness in terms of stylolite types, with seismogram pinning ones being the thickest while suture and sharp peak ones being the thinnest.

The percentage of filling by insoluble material along stylolites is almost the same for rectangular layer and seismogram pinning-type stylolites and is lower for suture and sharp peak and wave-like stylolite types but with significantly higher variability in the latter cases. Regarding rock textures, the highest amount of insoluble material corresponds to wackestones, while stylolites hosted in the other textures collected slightly fewer insolubles.

The maximum stylolite spacing corresponds to mudstones and grainstones, followed by wackestones. This supports the idea that heterogeneity in grain size, grain sorting and composition controls stylolite formation. Stylolite spacing progressively increases from the rectangular layer to the wave-like stylolite types.

The analysis of the degree of stylolite connectivity reveals that samples with stylolite networks (i.e., connected stylolites) are the most abundant, followed by those with isolated ones. It is worth noting that the scale of analysis used (restricted to that of a thin section) can influence the results of stylolite connectivity.

Author Contributions: Conceptualization, S.M., J.D.M.-M., P.D.B. and E.G.-R.; methodology, S.M., J.D.M.-M., P.D.B. and E.G.-R.; formal analysis, S.M.; investigation, S.M., J.D.M.-M., P.D.B. and E.G.-R.; resources, S.M., J.D.M.-M. and E.G.-R.; data curation, S.M.; writing—original draft preparation, S.M.; writing—review and editing, S.M., J.D.M.-M., P.D.B. and E.G.-R.; visualization, S.M., J.D.M.-M., P.D.B. and E.G.-R.; supervision, J.D.M.-M. and E.G.-R.; project administration, J.D.M.-M. and E.G.-R.; funding acquisition, J.D.M.-M. and E.G.-R. All authors have read and agreed to the published version of the manuscript.

Funding: This research was funded by the Spanish Ministry of Science and Innovation (MCIN)/State Research Agency of Spain (AEI)/10.13039/501100011033 (project number PID2020-118999GBI00), MCIN/AEI/10.13039/501100011033/FEDER-EU (project number PID2021-12246NB-C22), MCIN/AEI/10.13039/501100011033/European Social Fund—Investing in Your Future (Ramón y Cajal fellowship RyC-2018-026335-I to E.G.R) and MCIN/AEI/10.13039/501100011033/European Union NextGenerationEU/PRTR (project number CNS2023–145382) and the Agència de Gestió d'Ajuts Universitaris i de Recerca (grant to Consolidated Research Group Geologia Sedimentària 2021 SGR 00349).

Data Availability Statement: The original contributions presented in the study are included in the article. Further inquiries can be directed to the corresponding author.

Acknowledgments: The authors are grateful to Małgorzata Kozłowska, University of Warsaw, for helping collect some of the photos of Figures 3 and 4, and to Cees W. Passchier for discussions, suggestions and for reviewing the manuscript before submission. The authors are grateful to the anonymous reviewers and editors for their constructive comments and suggestions, which have helped improve the quality of this study.

Conflicts of Interest: The authors declare no conflicts of interest. The funders had no role in the design of the study; in the collection, analyses or interpretation of data; in the writing of the manuscript; or in the decision to publish the results.

References

1. Stockdale, P.B. *Stylolites: Their Nature and Origin*; Indiana University Studies: Bloomington, IN, USA, 1922; Volume 9, pp. 1–97.
2. Railsback, L.B. Lithologic controls on morphology of pressure-dissolution surfaces (stylolites and dissolution seams) in Paleozoic carbonate rocks from the Mid Eastern United-States. *J. Sediment. Res.* **1993**, *63*, 513–522. [CrossRef]
3. Touissant, R.; Aharonov, E.; Koehn, D.; Gratier, J.P.; Ebner, M. Stylolites: A review. *J. Struct. Geol.* **2018**, *114*, 163–195. [CrossRef]
4. Rawnling, G.C.; Godwin, L.B.; Wilson, J.L. Internal architecture, permeability structure, and hydrologic significance of contrasting fault-zone types. *Geology* **2001**, *29*, 43–46. [CrossRef]
5. Rolland, A.; Toussaint, R.; Baud, P.; Schmittbuhl, J.; Conil, N.; Koehn, D.; Renard, F.; Gratier, J.P. Modeling the growth of stylolites in sedimentary rocks. *J. Geophys. Res* **2012**, *117*, B06403. [CrossRef]
6. Dunnington, H.V. Stylolite development post-dates rock induration. *J. Sediment. Petrol.* **1954**, *24*, 27–49. [CrossRef]
7. Koepnick, R.B. Distribution and Permeability of Stylolite-Bearing Horizons Within a Lower Cretaceous Carbonate Reservoir in the Middle East. *SPE Form Eval* **1987**, *2*, 137–142. [CrossRef]
8. Gratier, J.-P.; Muquet, L.; Hassani, R.; Renard, F. Experimental microstylolites in quartz and modeled application to natural stylolitic structures. *J. Struct. Geol.* **2005**, *27*, 89–100. [CrossRef]
9. Ben-Itzhak, L.L.; Aharonov, E.; Karcz, Z.; Kaduri, M.; Toussaint, R. Sedimentary stylolite networks and connectivity in limestone: Large-scale field observations and implications for structure evolution. *J. Struct. Geol.* **2014**, *63*, 106–123. [CrossRef]
10. Liu, M.; Fang, C.; Chen, D. Syndepositional and diagenetic processes in the pigmentation of Middle Ordovician carbonate red beds in South China. *Sediment. Geol.* **2024**, *470*, 106722. [CrossRef]
11. Nelson, R.A. Significance of fracture sets associated with stylolite zones. *Am. Assoc. Pet. Geol. Bull.* **1981**, *65*, 2417–2425.
12. Dutton, S.P.; Willis, B.J. Comparison of outcrop and subsurface sandstone permeability distribution, lower cretaceous Fall River formation, South Dakota and Wyoming. *J. Sediment. Res.* **1998**, *68*, 890–900. [CrossRef]
13. Alsharhan, A.; Sadd, J.L. Stylolites in Lower Cretaceous carbonate reservoirs. *U.A.E: Soc. Sediment. Geol. Spec. Publ.* **2000**, *69*, 185–207.
14. Wong, P.K.; Oldershaw, A. Burial cementation in the Devonian, Kaybob Reef complex, Alberta, Canada. *J. Sediment. Pet.* **1981**, *51*, 507–520.
15. Tada, R.; Siever, R. Pressure Solution during Diagenesis. *Annu. Rev. Earth Planet. Sci.* **1989**, *17*, 89–118. [CrossRef]
16. Finkel, E.A.; Wilkinson, B.H. Stylolitization as Source of cement in Mississippian Salem Limestone, West-Central Indiana. *Am. Assoc. Pet. Geol. Bull.* **1990**, *74*, 174–186.
17. Ehrenberg, S.N.; Morad, S.; Yaxin, L.; Chen, R. Stylolites and porosity in a lower Cretaceous limestone reservoir, onshore Abu Dhabi, UAE. *J. Sediment. Res.* **2016**, *86*, 1228–1247. [CrossRef]
18. Heap, M.J.; Baud, P.; Reuschlé, T.; Meredith, P.G. Stylolites in limestones: Barriers to fluid flow? *Geology* **2014**, *42*, 51–54. [CrossRef]
19. Heap, M.; Reuschle, T.; Baud, P.; Renard, F.; Iezzi, G. The permeability of stylolite Bearing limestone. *J. Struct. Geol.* **2018**, *116*, 81–93. [CrossRef]
20. Paganoni, M.; Al Harthi, A.; Morad, D.; Morad, S.; Ceriani, A.; Mansurbeg, H.; Al Suwaidi, A.; Al-Aasm, I.S.; Ehrenberg, S.N.; Sirat, M. Impact of stylolitization diagenesis of a Lower Cretaceous carbonate reservoir from a giant oilfield, Abu Dhabi, United Arab Emirates. *Sediment. Geol.* **2016**, *335*, 70–92. [CrossRef]
21. Bruna, P.O.; Lavenu, A.P.; Matonti, C.; Bertotti, G. Are stylolites fluid-flow efficient features? *J. Struct. Geol.* **2019**, *125*, 270–277. [CrossRef]
22. Martín-Martín, J.D.; Gomez-Rivas, E.; Gomez-Gras, D.; Travé, A.; Ameneiro, R.; Koehn, D.; Bons, P.D. Activation of stylolites as conduits for overpressured fluid flow in dolomitized platform carbonates. *Geol. Soc. Lond. Spec. Publ.* **2018**, *459*, 157–176. [CrossRef]

23. Gomez-Rivas, E.; Martín-Martín, J.D.; Bons, P.D.; Koehn, D.; Griera, A.; Travé, A.; Llorens, M.G.; Humphrey, E.; Neilson, J. Stylolites and stylolite networks as primary controls on the geometry and distribution of carbonate diagenetic alterations. *Mar. Pet. Geol.* **2022**, *136*, 105444. [CrossRef]
24. Rashid, F.; Glover, P.W.J.; Lorinczi, P.; Hussein, D.; Lawrence, J.A. Microstructural controls on reservoir quality in tight oil carbonate reservoir rocks. *J. Pet. Sci. Eng.* **2017**, *156*, 814–826. [CrossRef]
25. Kaveh-Ahangar, S.; Nozaem, R.; Tavakoli, V. The effects of planar structures on reservoir quality of Triassic Kangan formation in the central Persian Gulf, an integrated approach. *J. Afr. Earth Sci.* **2023**, *197*, 104764. [CrossRef]
26. Guzzetta, G. Kinematics of stylolite formation and physics of pressure-solution process. *Tectonophysics* **1984**, *101*, 383–394. [CrossRef]
27. Park, W.C.; Schot, E.H. Stylolites: Their nature and origin. *J. Sediment. Petrol.* **1968**, *38*, 175–191.
28. Vandeginste, V.; John, C.M. Diagenetic implications of stylolitization in pelagic carbonates, Canterbury basin, offshore New Zealand. *J. Sediment. Res.* **2013**, *83*, 226–240. [CrossRef]
29. Koehn, D.; Rood, M.P.; Beaudoin, N.; Chung, P.; Bons, P.D.; Gomez-Rivas, E. A new stylolite classification scheme to estimate compaction and local permeability variations. *Sediment. Geol.* **2016**, *346*, 60–71. [CrossRef]
30. Humphrey, E.; Gomez-Rivas, E.; Neilson, J.; Martín-Martín, J.D.; Healy, D.; Yao, S.; Bons, P.D. Quantitative analysis of stylolite networks in different platform carbonate facies. *Mar. Pet. Geol.* **2020**, *114*, 104203. [CrossRef]
31. Beaudoin, N.; Koehn, D.; Lacombe, O.; Lecouty, A.; Billi, A.; Aharonov, E.; Parlangeau, C. Fingerprinting stress: Stylolite and calcite twinning paleopiezometry revealing the complexity of progressive stress patterns during folding-the case of the Monte Nero anticline in the Apennines, Italy. *Tectonics* **2016**, *35*, 1687–1712. [CrossRef]
32. Wu, J.; Fan, T.; Gomez-Rivas, E.; Travé, A.; Gao, Z.; Kang, Z.; Koehn, D.; Bons, P.D. Relationship between stylolite morphology and the sealing potential of stylolite-bearing carbonate cap rocks. *Geol. Soc. Am. Bull.* **2023**, *135*, 689–711. [CrossRef]
33. Wanless, H.R. Limestone response to stress: Pressure solution and dolomitization. *J. Sediment. Res.* **1979**, *49*, 437–462.
34. Rustichelli, A.; Tondi, E.; Korneva, I.; Baud, P.; Vinciguerra, S.; Agosta, F.; Reuschlé, T.; Janiseck, J.M. Bedding-parallel stylolites in shallow-water limestone successions of the Apulian Carbonate Platform (central-southern Italy). *Ital. J. Geosci.* **2015**, *134*, 513–534. [CrossRef]
35. Ben-Itzhak, L.L.; Aharonov, E.; Toussaint, R.; Sagy, A. Upper bound on stylolite roughness as indicator for amount of dissolution. *Earth Planet. Sci. Lett.* **2012**, *337*, 186–196. [CrossRef]
36. Renard, F.; Schmittbuhl, J.; Gratier, J.-P.; Meakin, P.; Merino, E. Three Dimensional roughness of stylolites in limestones. *J. Geophys. Res. Solid Earth* **2004**, *109*, B03209. [CrossRef]
37. Hickman, S.H.; Evans, B. Experimental pressure solution in halite: The effect of grain interphase boundary structure. *J. Geol. Soc.* **1991**, *148*, 549–560. [CrossRef]
38. Renard, F.; Dysthe, D.; Feder, J.; Bjorlykke, K.; Jamtveit, B. Enhanced pressure solution creep rates induced by clay particles: Experimental evidence in salt aggregates. *Geophys. Res. Lett.* **2001**, *28*, 1295–1298. [CrossRef]
39. Meyer, E.E.; Greene, G.W.; Alcantar, N.A.; Israelachvili, J.N.; Boles, J.R. Experimental investigation of the dissolution of quartz by a muscovite mica surface: Implications for pressure solution. *J. Geophys. Res. Solid Earth* **2006**, *111*, B08202. [CrossRef]
40. Greene, G.W.; Kristiansen, K.; Meyer, E.E.; Boles, J.R.; Israelachvili, J.N. Role of electrochemical reactions in pressure solution. *Geochim. Cosmochim. Acta* **2009**, *73*, 2862–2874. [CrossRef]
41. Morad, D.; Nader, F.H.; Morad, S.; Al Darmaki, F.; Hellevang, H. Impact of stylolitization on fluid flow and diagenesis in foreland basins: Evidence from an Upper Jurassic Carbonate gas reservoir, Abu Dhabi, United Arab Emirates. *J. Sediment. Res.* **2018**, *88*, 1345–1361. [CrossRef]
42. Koehn, D.; Renard, F.; Toussaint, R.; Passchier, C.W. Growth of stylolite teeth patterns depending on normal stress and finite compaction. *Earth Planet. Sci. Lett.* **2007**, *257*, 582–595. [CrossRef]
43. Koehn, D.; Ebner, M.; Renard, F.; Toussaint, R.; Passchier, C.W. Modelling of stylolite geometries and stress scaling. *Earth Planet. Sci. Lett.* **2012**, *341*, 104–113. [CrossRef]
44. Ebner, M.; Koehn, D.; Toussaint, R.; Renard, F. The influence of rock heterogeneity on the scaling properties of simulated and natural stylolites. *J. Struct. Geol.* **2009**, *31*, 72–82. [CrossRef]
45. Chambon, G.; Schmittbuhl, J.; Cordfir, A.; Orellana, N.; Diraiso, M.; Geraud, Y. The thickness of faults: From laboratory experiments to field scale observations. *Tectonophysics* **2006**, *426*, 77–94. [CrossRef]
46. Gratier, J.-P.; Richard, J.; Renard, F.; Mittempergher, S.; Doan, M.L.; Di Toro, G.; Hadizadeh, J.; Boullier, A.M. Aseismic sliding of active faults by pressure solution creep: Evidence from the San Andreas Fault Observatory at Depth. *Geology* **2011**, *39*, 1131–1134. [CrossRef]
47. Rolland, A.; Toussaint, R.; Baud, P.; Conil, N.; Landrein, P. Morpholofical analysis of stylolites for paleostress estimation in limestones. *Int. J. Rock Mech. Min. Sci.* **2014**, *67*, 212–225. [CrossRef]
48. Bathrust, R.G.C. Diagenetic enhanced bedding in argillaceous platform limestones: Stratified cementation and selective compaction. *Sedimentology* **1971**, *34*, 749–778. [CrossRef]

49. Buxton, T.; Sibbley, D.F. Pressure Solution Features in a shallow buried limestone. *J. Sediment. Petrol.* **1981**, *51*, 19–26. [CrossRef]
50. Braithwaite, C.J.R. Mechanically induced stylolites and loss of porosity in dolomites. *J. Pet. Geol.* **1986**, *9*, 343–348. [CrossRef]
51. Walderhaug, O.; Bjorkum, P.A.; Aase, N. Kaolini-coating of stylolites, effect on quartz cementation and general implications for dissolution at mineral interfaces. *J. Sediment. Res.* **2006**, *73*, 234–243. [CrossRef]
52. Angheluta, L.; Mathiesen, J.; Aharanow, E. Compaction of Porous rocks by dissolution on discrete stylolites: A one dimensional model. *Journal of Geophysical Research-Atmospheres* **2012**, *117*, B08203. [CrossRef]
53. Railsback, L.B. Evaluation of spacing of stylolites and its implications for self-organization of pressure dissolution. *J. Sediment. Res.* **1998**, *68*, 2–7. [CrossRef]
54. Gratier, J.-P.; Guiguet, R.; Renard, F.; Jenatton, L.; Bernard, D. A pressure solution creep law for quartz from indentation experiments. *J. Geophys. Res. Solid Earth* **2009**, *114*, B03403. [CrossRef]
55. Mardon, D. Localized Pressure Solution and the Formation of Discrete Solution Seams. Ph.D. Thesis, Texas A&M University, College Station, TX, USA, 1988; p. 246.
56. Fletcher, R.C.; Pollard, D.D. Anti-Crack Model for Pressure Solution Surfaces. *Geology* **1981**, *9*, 419–424. [CrossRef]
57. Safaricz, M.; Davison, I. Pressure solution in chalk. *Am. Assoc. Pet. Geol. Bull.* **2005**, *89*, 383–401. [CrossRef]
58. Aharonov, E.; Katsman, R. Interaction between Pressure Solution and Clays in Stylolite Development: Insights from Modeling. *Am. J. Sci.* **2009**, *309*, 607–632. [CrossRef]
59. Levenson, Y.; Schiller, M.; Kreisserman, Y.; Emmanuel, S. Calcite dissolution rates in texturally diverse calcareous rocks. In *Fundamental Controls on Fluid Flow in Carbonates: Current Workflows to Emerging Technologies*; Agar, S.M., Geiger, S., Eds.; Geological Society, London, Special Publications: London, UK, 2014; Volume 4.6, pp. 81–94.
60. Benedicto, A.; Schultz, R.A. Stylolites in limestone: Magnitude of contractional strain accommodated and scaling relationships. *J.'Struct. Geol.* **2010**, *32*, 1250–1256. [CrossRef]
61. Nenna, F.A.; Aydin, A. The formation and growth of pressure solution seams in clastic rocks: A field and analytical study. *J. Struct. Geol.* **2011**, *33*, 633–643. [CrossRef]
62. Dunham, R.J. Classification of carbonate rocks according to depositional texture. In *Classification of Carbonate Rocks*; Ham, W.E., Ed.; American Association of Petroleum Geologists: Tulsa, OK, USA, 1962; pp. 108–121.
63. Tondi, E.; Antonellini, M.; Aydin, A.; Marchegiani, L.; Cello, G. The role of deformation bands, stylolites and sheared stylolites in fault development in carbonate grainstones of Majella Mountain, Italy. *J. Struct. Geol.* **2006**, *28*, 376–391. [CrossRef]
64. Bjorkum, P.A. How important is pressure in causing dissolution of quartz in sandstones? *J. Sediment. Res.* **1996**, *66*, 147–154.
65. Kristiansen, K.; Valtiner, M.; Greene, G.W.; Boles, J.R.; Israelachvili, J.N. Pressure solution—The importance of the electrochemical surface potentials. *Geochim. Cosmochim. Acta* **2011**, *75*, 6882–6892. [CrossRef]
66. Harris, N.B. Low-Porosity Haloes at Stylolites in the Feldspathic Upper Jurassic Ula Sandstone, Norwegian North Sea: An Integrated Petrographic and Chemical Mass-Balance Approach. *J. Sediment. Res.* **2006**, *76*, 444–459. [CrossRef]
67. Heald, M.T. Significance of stylolites in permeable sandstones. *J. Sediment. Res.* **1959**, *29*, 251–253.
68. Carozzi, A.V.; Vonbergen, D. Stylolitic Porosity in Carbonates—A Critical Factor for Deep Hydrocarbon Production. *J. Pet. Geol.* **1987**, *10*, 267–282. [CrossRef]
69. Van Geet, M.; Swennen, R.; Wevers, M. Towards 3-D petrography: Application of microfocus computer tomography in geological science. *Comput. Geosci.* **2001**, *27*, 1091–1099. [CrossRef]
70. Ebner, M.; Piazolo, S.; Renard, F.; Koehn, D. Stylolite interfaces and surrounding matrix material: Nature and role of heterogeneities in roughness and microstructural development. *J. Struct. Geol.* **2010**, *32*, 1070–1084. [CrossRef]
71. Walderhaug, O.; Bjorkum, P.A. The effect of stylolite spacing on quartz cementation in the Lower Jurassic Stø Formation, southern Barents Sea. *J. Sediment. Res.* **2003**, *73*, 146–156. [CrossRef]
72. Emmanuel, S.; Ague, J.J. Modeling the impact of nano-pores on mineralization in sedimentary rocks. *Water Resour. Res.* **2009**, *45*, W04406. [CrossRef]
73. Emmanuel, S.; Ague, J.J.; Walderhaug, O. Interfacial energy effects and the evolution of pore size distributions during quartz precipitation in sandstone. *Geochim. Cosmochim. Acta* **2010**, *74*, 3539–3552. [CrossRef]
74. Wu, J.; Fan, T.L.; Gomez-Rivas, E.; Gao, Z.Q.; Yao, S.Q.; Li, W.H.; Zhang, C.J.; Sun, Q.Q.; Gu, Y.; Xiang, M. Impact of pore structure and fractal characteristics on the sealing capacity of Ordovician carbonate cap rock in the Tarim Basin China. *Mar. Pet. Geol.* **2019**, *102*, 557–579. [CrossRef]
75. Wu, J.; Fan, T.; Gu, Y.; Gao, Z. Identification and characteristic analysis of carbonate cap rock: A case study from the Lower-Middle Ordovician Yingshan Formation in Tahe oilfield, Tarim Basin China. *J. Pet. Sci. Eng.* **2018**, *164*, 362–381. [CrossRef]
76. Tucker, M.E.; Wright, V.P. *Carbonate Sedimentol*; John Wiley and Sons: Hoboken, NJ, USA, 2009; pp. 1–14.
77. Thomson, A. Pressure solution and porosity. *Soc. Econ. Paleontol. Mineral. Spec. Publ.* **1959**, *7*, 92–110.
78. Alcantar, N.; Israelachvili, J.; Boles, J. Forces and ionic transport between mica surfaces: Implications for pressure solution. *Geochim. Cosmochim. Acta* **2003**, *67*, 1289–1304. [CrossRef]

79. Gratier, J.P.; Noiriel, C.; Renard, F. Experimental evidence for rock layering development by pressure solution. *Geology* **2015**, *27*, 89–100. [CrossRef]
80. Humphrey, E.; Gomez-Rivas, E.; Koehn, D.; Bons, P.D.; Neilson, J.; Martín-Martín, J.D.; Schoenherr, J. Stylolite-controlled diagenesis of a mudstone carbonate reservoir: A case study from the Zechstein_2_Carbonate (Central European Basin, NW Germany). *Mar. Pet. Geol.* **2019**, *109*, 88–107. [CrossRef]
81. Zeeb, C.; Gomez-Rivas, E.; Bons, P.D.; Blum, P. Evaluation of sampling methods for fracture network characterization using outcrops. *Am. Assoc. Pet. Geol. Bull.* **2013**, *97*, 1545–1566. [CrossRef]
82. Merino, E.; Ortoleva, P.; Strickholm, P. Generation of evenly-spaced pressure solution seams during (late) diagenesis: A kinetic theory. *Contrib. Mineral. Petrol.* **1983**, *82*, 360–370. [CrossRef]
83. Karcz, Z.; Aharonov, E.; Ertas, D.; Polizzotti, R.; Scholz, C.H. Deformation by dissolution and plastic flow of a single crystal sodium chloride indenter: An experimental study under the confocal microscope. *J. Geophys. Res. Solid Earth* **2008**, *113*, B04205. [CrossRef]
84. Wangen, M. Modeling porosity evolution and cementation of sandstones. *Mar. Pet. Geol.* **1998**, *15*, 453–465. [CrossRef]